

Capacity and Efficiency Improvement of MIMO Antenna Systems for 5G Handheld Terminals

Ahmad H. Abdelgwad^{1, 2, *} and Mohammad Ali³

Abstract—The efficacy of including a defected ground structure (DGS) for mobile communication on a mobile phone PCB in improving the multiple input multiple output (MIMO) system performance is evaluated and demonstrated in the context of single and multiple-element two-port planar inverted-F antennas (PIFAs). The proposed scheme designed and developed for operation in the 3.5 GHz long term evolution (LTE) and future 5G frequency bands demonstrates efficiency improvement by 15% and capacity improvement by around 7% because of the significant reduction in mutual coupling between the antenna ports. Results in free space as well as next to a human head and hand phantom are presented.

1. INTRODUCTION

Mobile wireless communications have seen tremendous growths in the last decades in the form of smart mobile phones, watches, wireless enabled personal digital assistants (PDAs), etc. To support the increasing demand in data, more spectrums have been made open for public use throughout the world including LTE (Long Term Evolution), AWS (Advanced Wireless Services), and mm-Wave systems.

In the device hardware front, significant research activities have been reported. Specifically, on the antenna design and development front, multi-antenna MIMO (Multiple Input Multiple Output) systems have become the most promising candidate to support the increased data demand [1–4]. The application of MIMO antennas on the device side also includes high performance Wi-Fi routers and other wireless devices.

One key challenge regarding multi-antenna MIMO systems for the handheld is to successfully accommodate multiple miniature platform integrated antennas on a small device [5–8]. Associated with that challenge comes undesirable increased mutual coupling [9–14], efficiency degradation, human body effects [15–17], etc. Thus, it is important to design and develop innovative methods and technologies to mitigate such effects so that MIMO system efficiency and capacity can be improved. That is the focus of this work.

A two-port planar inverted-F antenna (PIFA) with a slot on the ground plane between the feeding ports was introduced in [18] which achieved around 14 dB isolation at 2.45 GHz. Recently, Chattha in [19] has used a two-port PIFA to propose a four-port two-element MIMO antenna. However, the configuration with a slot on the ground for a two-port PIFA has a deficiency that the isolation obtained between the ports is rather limited, i.e., less than 15 dB. Isolation improvement more than what was achieved in [18, 19] which has significant MIMO performance improvement potentials. The above studies do not investigate system level diversity and MIMO performance, such as EDG (Effective Diversity Gain), CDF (Cumulative Density Functions), and system capacity.

Received 21 May 2020, Accepted 6 August 2020, Scheduled 21 August 2020

* Corresponding author: Ahmed H. Abdelgwad (ahmedha@email.sc.edu).

¹ Department of Electrical Engineering, University of South Carolina, Columbia, SC 29208, USA. ² Department of Electrical Engineering, Fayoum University, Fayoum 63514, Egypt. ³ Department of Electrical Engineering, University of South Carolina, Columbia, SC 29208, USA.

In this paper, we design, develop, and integrate a DGS to significantly increase the isolation and efficiency of a two-port multi-antenna MIMO system for a handheld device. To demonstrate the efficacy of the proposed approach, we compare and contrast among four antenna configurations and show that the DGS based design is capable of higher efficiency. As a result, the proposed scheme provides higher capacity (bps/Hz) than the other cases. Studies in the presence of a human head and hand model are also presented to indicate improved performance.

The paper is organized as follows. First, in order to fully understand and appreciate the performance of multi-antenna MIMO systems for the handheld, the fundamental mathematical relationships are defined based on information available from the literature. Followed by that, we present the geometrical configurations of the various antenna plus DGS configurations. Third, results of scattering parameters, radiation pattern, and efficiency are presented followed by CDF (Cumulative Density Function) and capacity. Finally, the effects on the performance of the proposed MIMO antenna scheme are evaluated in the presence of a human's hand and head.

2. CRITERIA TO EVALUATE DIVERSITY/MIMO ANTENNA PERFORMANCE

Several important diversity/MIMO antenna performance parameters that have been used in this paper are defined below.

2.1. Initial Parameters

The mean effective gain (MEG) of the i th element of a multi-antenna system can be calculated using [20]

$$\text{MEG}_i = \iint \left\{ \frac{\Gamma}{1+\Gamma} G_\theta(\Omega) P_\theta(\Omega) + \frac{1}{1+\Gamma} G_\phi(\Omega) P_\phi(\Omega) \right\} d\Omega \quad (1)$$

where Γ is the cross polarization power ratio which is defined as the ratio of the average incident power corresponding to the vertical and horizontal polarizations, e.g., $\Gamma = P_V/P_H$; $G_\theta(\Omega)$ and $G_\phi(\Omega)$ are the θ and ϕ components of the antenna power gain patterns, respectively; $P_\theta(\Omega)$ and $P_\phi(\Omega)$ are the θ and ϕ components of the angular density functions of the incoming plane waves, respectively; and $d\Omega$ is the differential of the beam solid angle given by $d\Omega = \sin\theta d\theta d\phi$.

By considering a uniform propagation environment with $\Gamma = 1$ and $P_\theta = P_\phi = 1/4\pi$, as described in [21], the MEG was calculated as

$$\text{MEG}_i = \frac{e_{\text{tot}}^i}{2} = \frac{e_{\text{rad}}^i \cdot e_{\text{mis}}^i}{2} \quad (2)$$

where e_{tot}^i is the total efficiency of the i th antenna element defined as the product of its radiation efficiency, e_{rad}^i , and mismatch efficiency, e_{mis}^i , where

$$e_{\text{mis}}^i = 1 - \sum_{j=1}^N |S_{ij}|^2 \quad (3)$$

The *Envelope Correlation Coefficient (ECC)* and the cross-correlation coefficient, ρ_{cij} , were calculated as [22, 23]

$$\text{ECC}_{ij} \cong |\rho_{cij}|^2 \quad (4)$$

where

$$\rho_{cij} = \frac{\iint A_{ij}(\Omega) d\Omega}{\sqrt{\iint A_{ii}(\Omega) d\Omega \cdot \iint A_{jj}(\Omega) d\Omega}} \quad (5)$$

where

$$A_{ij} = \text{XPRE}_{\theta,i}(\Omega) E_{\theta,j}^*(\Omega) P_\theta(\Omega) + E_{\Phi,i}(\Omega) E_{\Phi,j}^*(\Omega) P_\phi(\Omega) \quad (6)$$

where $E_\theta(\Omega)$ and $E_\phi(\Omega)$ are the θ and ϕ components of the antenna electric far-field gain patterns, respectively. For comparison and elucidation, ρ_{cij} was also estimated using the antenna S -parameters [24]

$$\rho_{cij} = \frac{-\sum_{n=1}^N S_{ni}^* S_{nj}}{\sqrt{\left(1 - \sum_{n=1}^N |S_{ni}|^2\right) \left(1 - \sum_{n=1}^N |S_{nj}|^2\right)}} \quad (7)$$

Note that Eq. (7) is only applicable when the antenna efficiency is high.

2.2. Diversity/MIMO Performance Parameters

In this work, a performance parameter called diversity antenna gain (DAG) [25] which is equivalent to effective diversity gain (EDG) [21] is used to evaluate the diversity performance of the proposed antennas

$$\text{DAG} = \text{EDG} = \frac{P_{\text{div}}}{P_{\text{inc OP\%}}} \quad (8)$$

where P_{div} is the combined signal power received by the multi-antenna system, and P_{inc} is the total incident power that can be received by a dual-polarized isotropic antenna with unit efficiency [20]. The values of P_{div} and P_{inc} are estimated at the same outage probability level, OP%, in a cumulative density function (CDF) of relative signal-to-noise-ratio (SNR) which is given by [21, 25]

$$\text{CDF} = P(P_{\text{div}} \leq x) = 1 - \frac{\sum_{i=1}^N \lambda_i^{N-1} e^{-x/\lambda_i}}{\prod_{j \neq i} (\lambda_i - \lambda_j)} \quad (9)$$

where λ are the eigenvalues of the covariance matrix, Λ , given by

$$\Lambda_{ij} = P_{\text{inc}} \cdot \sqrt{\text{MEG}_i \cdot \text{MEG}_j \cdot \text{ECC}_{ij}} \quad (10)$$

Finally, the MIMO system capacity of N transmitting and receiving antennas is calculated by [26–28]

$$C = E \left\{ \log_2 \left[\det \left(I_N + \frac{\gamma \cdot e_{\text{emb}}}{N} \Phi H H^H \right) \right] \right\} \quad (11)$$

where $E\{\cdot\}$ and $\det(\cdot)$ denote the expectation and determinant, respectively; I_N is an identity matrix; γ and e_{emb} refer to the SNR and the total embedded efficiency, respectively; H denotes the channel matrix while superscript H refers to the Hermitian (complex conjugate transpose); and Φ is the correlation matrix that is given for the two antenna system as follows

$$\Phi = \begin{bmatrix} 1 & \rho_{c12} \\ \rho_{c12}^* & 1 \end{bmatrix} \quad (12)$$

3. DEFINITIONS OF ANTENNA CONFIGURATIONS AND PARAMETERS

As indicated before, a PIFA with two ports was used as the element of choice to study and analyze our proposed multi-antenna system. By investigating the current flow between the ports, which increases the mutual coupling between them, it was found that the current primarily propagates through the ground plane instead of the radiating plate. Therefore, ground slots and planar defected ground structures are used to reduce the coupling between the ports.

In this work, four configurations are considered and designed for operation around 3.3 GHz to 3.6 GHz 5G band: (1) single element PIFA with a slotted ground (2) single element PIFA with a DGS ground (3) two-PIFAs with a slotted ground, and (4) two-PIFAs with a DGS ground. These configurations are depicted in Fig. 1. A 0.8 mm thick FR4 ($\epsilon_r = 4.4$ and $\tan \delta = 0.02$) Printed Circuit Board (PCB) board was used.

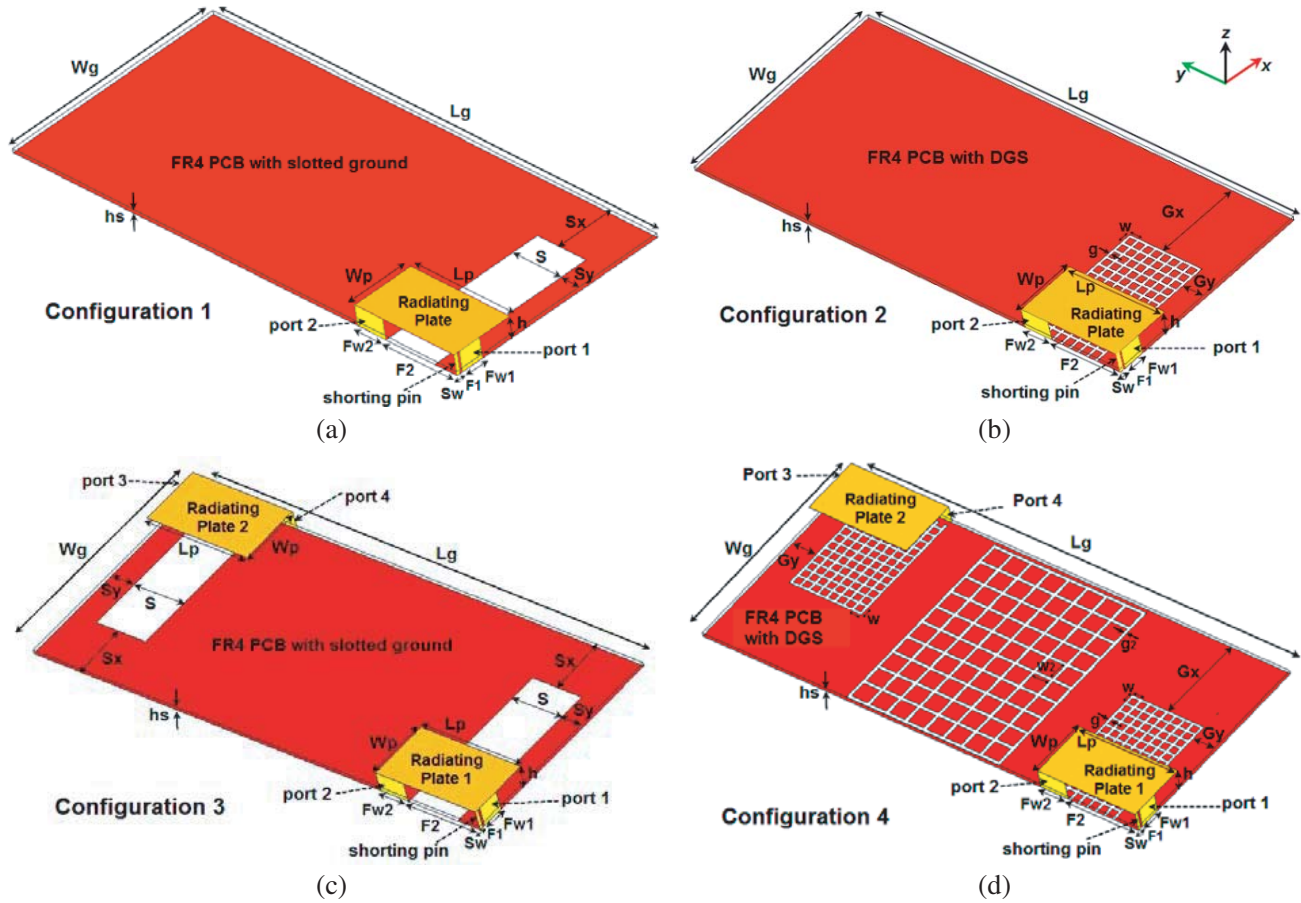


Figure 1. Configurations of the investigated multi-element antenna systems. (a) Single element PIFA with a slotted ground. (b) Single element PIFA with a DGS ground. (c) Two-PIFAs with a slotted ground. (d) Two-PIFAs with a DGS ground.

The proposed defected ground structure (Fig. 1(b)) was optimized by simulations using Ansys HFSS to achieve the highest isolation at 3.5 GHz. As shown in Fig. 1(b) for the DGS, there are more patches along the width direction of the ground. There are fewer patches along the length direction of the ground. Also, the number of patches to be accommodated along the length direction of the ground is restricted by the space between the two ports of the PIFA. If we refer the DGS length to be along the width of the ground plane, then that controls the frequency of the descending peak of the isolation vs. frequency response. From numerous simulations, it was observed that the length of the DGS was approximately half of the guided wavelength, λ_g corresponding to the frequency of the descending peak of the isolation vs. frequency characteristics curve. The guided wavelength is given by $\lambda_g = c/(f\sqrt{(\epsilon_r + 1)/2})$ where c is the velocity of light, and f is the operating frequency. For example, if there are 13 patches and 14 gaps with the patch to patch gap being g , then the length of the DGS = $13w + 14g$.

In general, the descending peak frequency does not depend on the number of patches along the ground width, patch width, or patch to patch gap. However, a larger number of smaller patches results in higher isolation. For instance, the isolation at 3.5 GHz is 20 dB, 32 dB, and 46 dB for $N = 6, 11,$ and 15, respectively, when the length of the DGS was fixed. The number of patches and the gap were optimized to achieve high isolation at 3.5 GHz while maintaining good return loss performance for the antenna ports. The optimized DGS dimensions along with the antenna parameters are listed in Table 1. The antenna structures were also fabricated and tested. Photographs of the fabricated antennas are shown in Fig. 2.

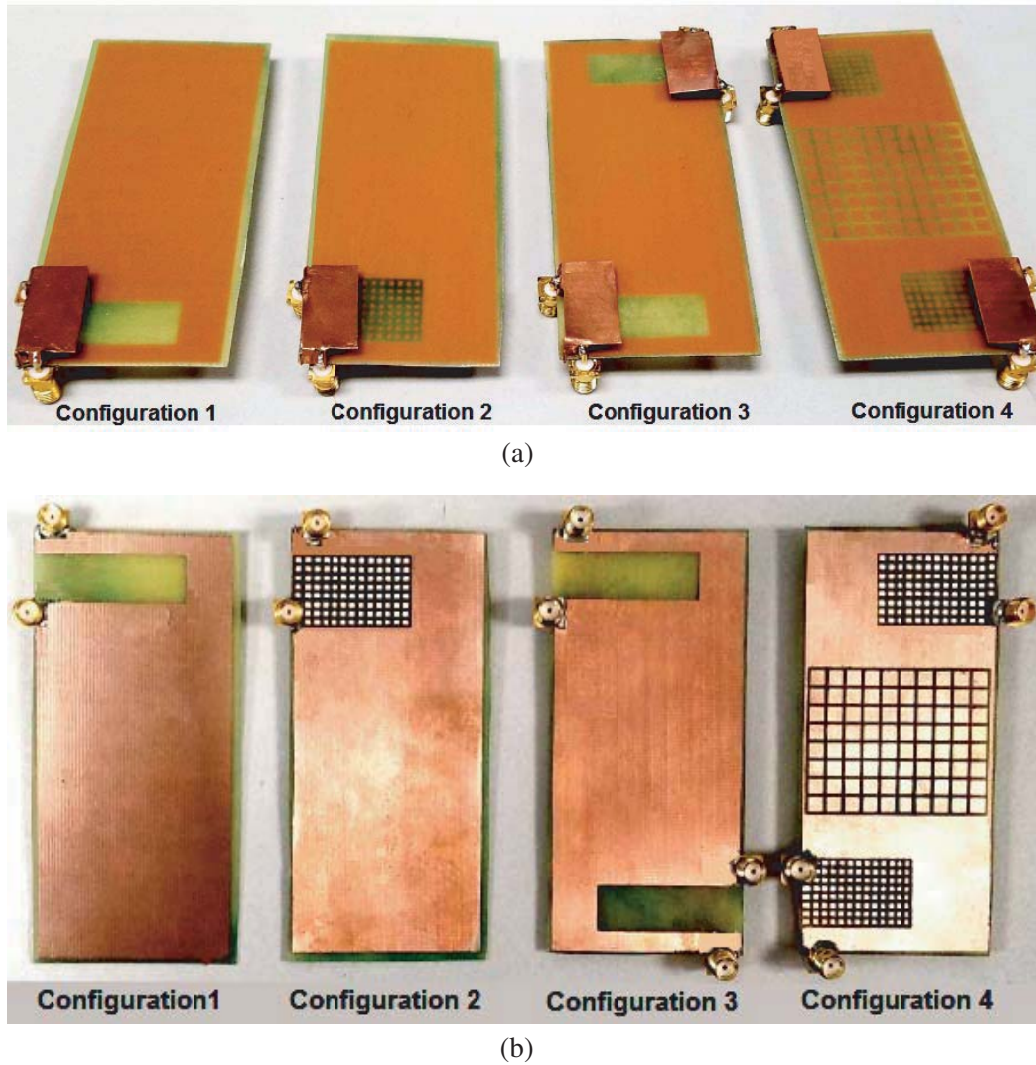


Figure 2. Fabricated MEA antenna structures. (a) Top view. (b) Bottom view.

4. ANTENNA PERFORMANCE RESULTS

The structures shown in Fig. 1 were simulated using Ansys HFSS, and they were measured using Agilent E5071C vector network analyzer (VNA). Prior to the measurement, the system imperfections were completely avoided by calibrating the VNA. Standard full 2 port calibration was performed using

Table 1. Optimized antenna configurations parameters.

Parameter	Value (mm)						
Lg	100.0	h	3.3	$F2$	16.10	g	0.6
Wg	45.0	Sw	0.7	S	11.00	Gx	17.8
hs	0.8	$Fw1$	4.5	Sx	11.00	Gy	5.5
Lp	22.4	$F1$	0.5	Sy	5.00	$w2$	3.6
Wp	12.6	$Fw2$	6.3	W	1.45	$g2$	0.7

open, short, 50-ohm load, and through connections. The calibration was then saved, and measurements were performed immediately after. At the measurement setup, the VNA dynamic range was 130 dB, and the noise floor was 0.004 dB rms at 70 kHz intermediate frequency bandwidth.

The simulated and measured scattering parameters S_{ii} of the proposed configurations are shown in Fig. 3. As seen, the minimum bandwidth achieved by all ports is about 600 MHz from around 3.2 GHz to 3.8 GHz for S_{ii} less than -10 dB. Simulated and measured center frequencies are nearly same for all cases. Difference between the simulated and measured responses lies in terms of the frequency range or bandwidth. It is normal for experimental S_{ii} to show somewhat broader bandwidth because it includes all losses and associated electromagnetic interference from the environment, materials in proximity, and the placement and routing of the VNA cables. Other sources for the differences could be probably due to the fabrication imperfections and the nonideality of FR4 material.

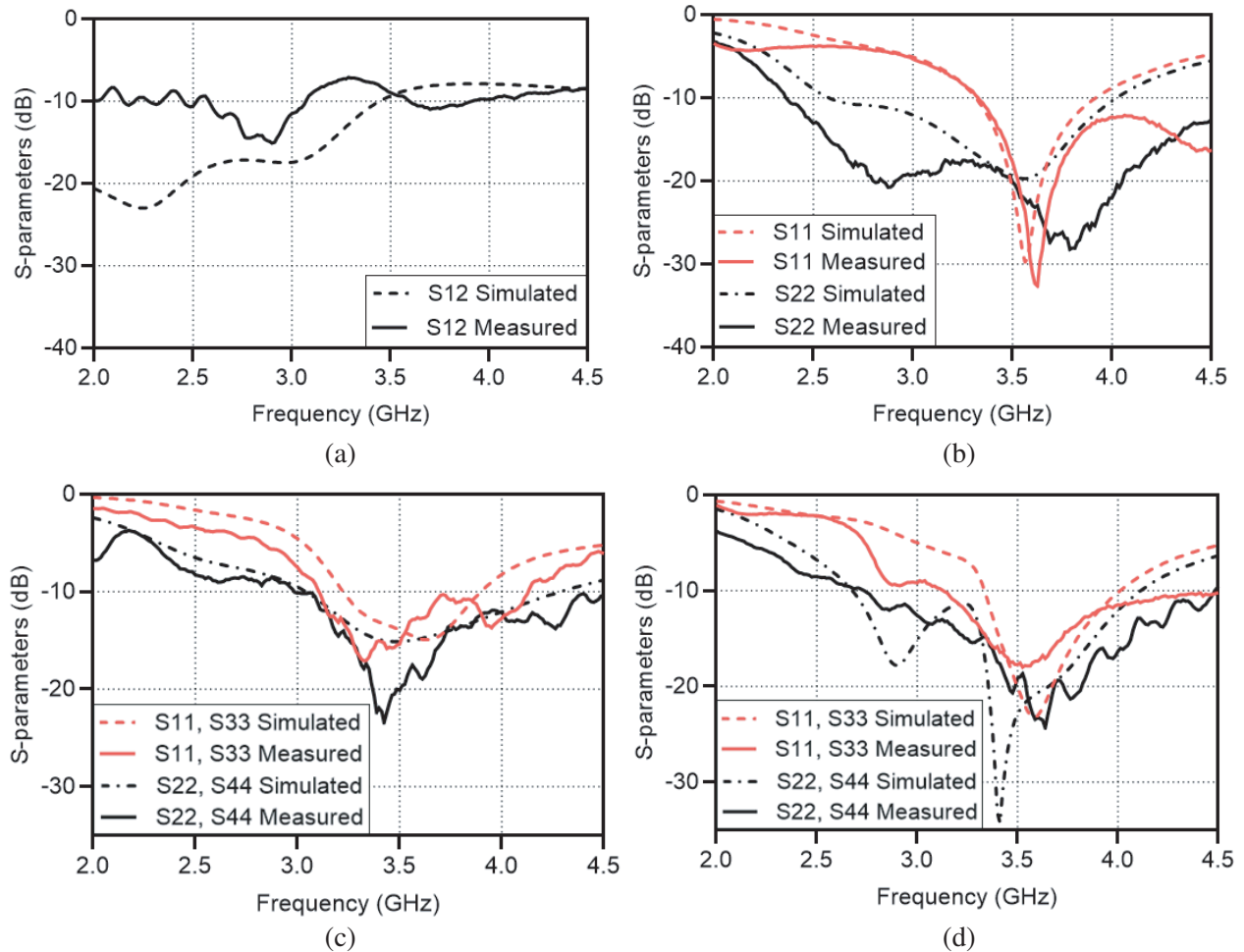


Figure 3. Magnitude of S_{ii} parameters of the studied MEA structures. (a) Configuration 1. (b) Configuration 2. (c) Configuration 3. (d) Configuration 4.

As indicated, the designed DGS was optimized to provide the lowest coupling between the ports at 3.5 GHz. Simulated and measured mutual coupling results for the various configurations are shown in Fig. 4. By investigating the current flow between the ports, which increases the mutual coupling between them, it was found that most of the current propagated through the ground plane compared to the radiating plates. As the ground current is the main contributor to the mutual coupling between ports, slots are etched on the ground plane in Configurations 1 and 3 to disturb the current flow between the feeding ports. In order to get further enhancement of the isolation, the ground plane is amended in

Configurations 2 and 4 by etching the DGS to chock the flow of current on the ground plane between the feeding ports. As seen, the simulated mutual coupling, S_{12} , at 3.5 GHz are -9 dB and -40 dB for Configuration 1 and Configuration 2, respectively. Average mutual coupling, S_{ij} , at 3.5 GHz is around -15 dB and -25 dB for Configuration 3 and Configuration 4, respectively. It should be noted that Configurations 2 and 4 are the ones with the DGS ground plane. This significant reduction of the mutual coupling can achieve better MIMO and diversity performance as the mutual coupling can seriously degrade the signal-to-interference-noise ratio (SINR) and the estimations of channel, carrier frequency offset, and angle of arrival. These adverse effects of mutual coupling are effectively reduced using the proposed EBG ground structure.

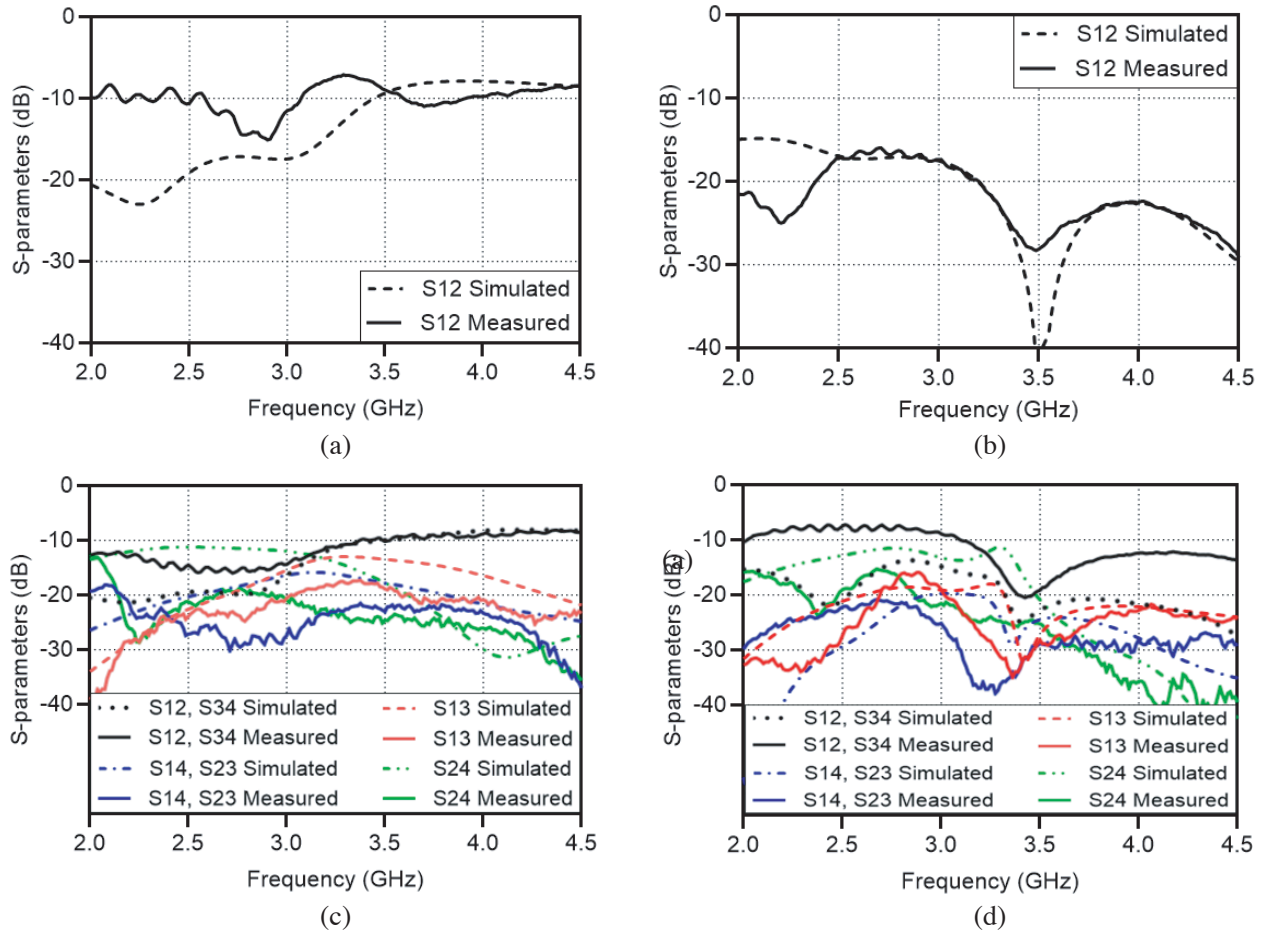


Figure 4. Mutual coupling, $|S_{ij}|$, of the studied MEA structures. (a) Configuration 1. (b) Configuration 2. (c) Configuration 3. (d) Configuration 4.

Simulated normalized realized gain patterns of ports are shown in Fig. 5 which show that the ports have distinctly different gain patterns exhibiting pattern diversity.

The total efficiency, e_{tot}^i , of each port and average values for each configuration were calculated. These efficiency data are illustrated in Fig. 6 which clearly reveal that the efficiencies of Configurations 2 and 4 (the ones with the DGSs) improved by around 15% compared to Configurations 1 and 3 (the ones without DGS), respectively. Since all ports of all antennas are well matched to their feed at 3.5 GHz (see Fig. 3), the efficiency improvement using the DGS can be mainly attributed to the significant reduction in the mutual coupling between the ports. The surface current distributions of the ground plane for the studied configurations at 3.5 GHz are shown in Fig. 7. As noted, the DGS prohibits the flow of current between ports which improves the isolation between them.

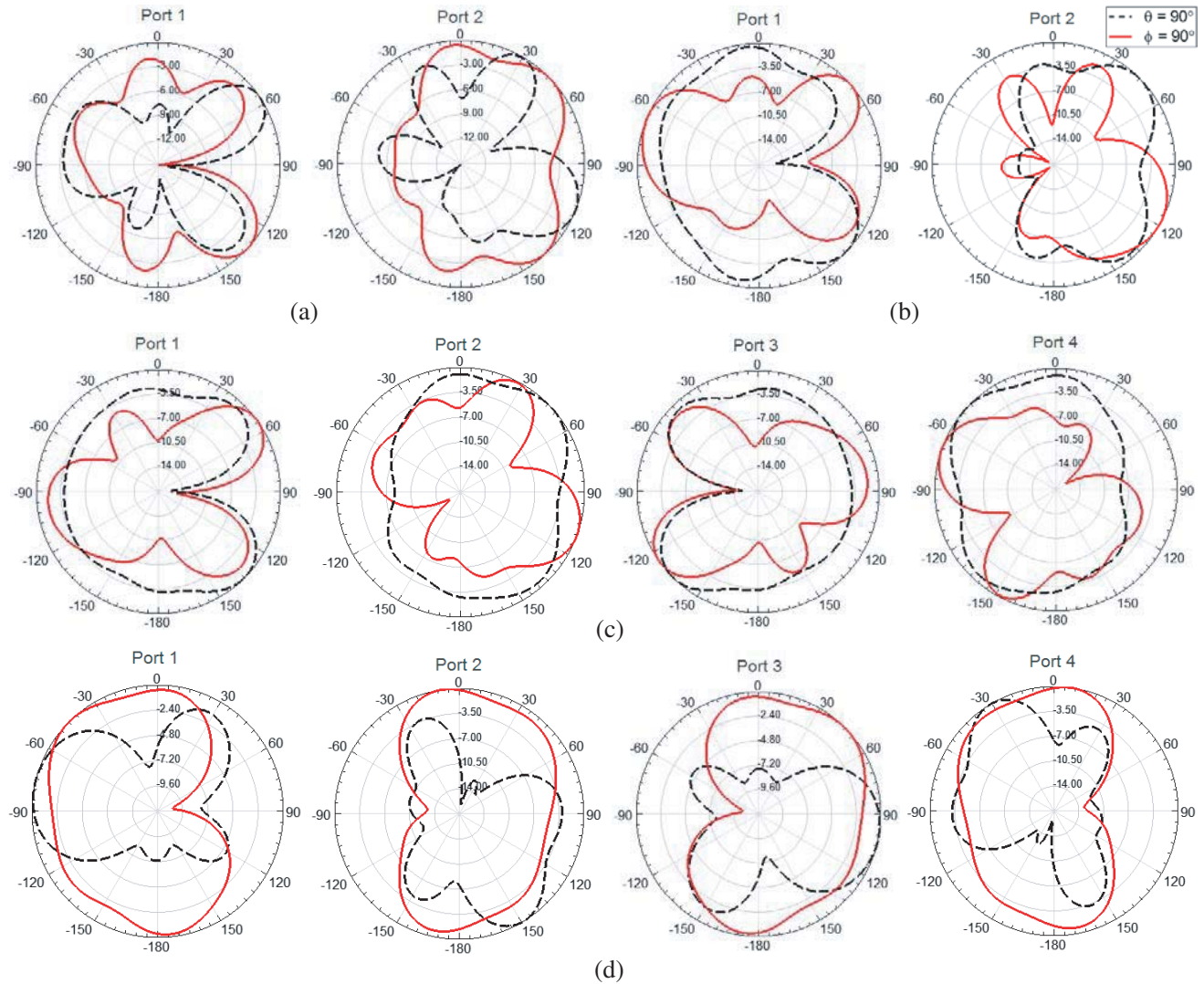


Figure 5. Normalized realized gain patterns in dB for the studied configurations. (a) Configuration 1. (b) Configuration 2. (c) Configuration 3. (d) Configuration 4.

5. DIVERSITY AND MIMO SYSTEM PERFORMANCE

The diversity and MIMO performance of the structures shown in Fig. 1 were also evaluated.

5.1. Diversity Performance

The MEG and ECC were calculated using both the scattering parameters and the radiation patterns and are listed in Table 2. All post-HFSS calculations were performed using MATLAB. As noted, the MEG values for the configurations with DGS ground (configurations 2 and 4) are higher than the ones without DGS ground (Configurations 1 and 3) because of the improvement of the ports' efficiencies. In addition, the ECC values for the DGS ground configurations are extremely low which confirm that the far-field patterns are uncorrelated because of the reduction of the mutual coupling between the ports. In order to observe the variations of MEG and ECC over the operating bandwidth, they are plotted versus frequency for Configuration 1 and Configuration 2 as shown in Fig. 8. As noted, Configuration 2 exhibits higher MEG values and lower ECC values than Configuration 1 because of the improvement of efficiency and isolation achieved by the DGS structure.

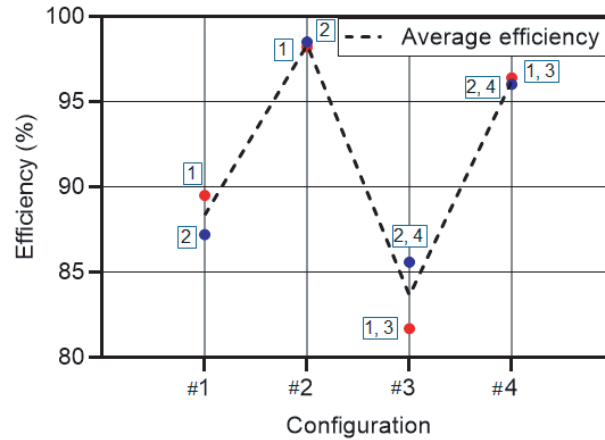


Figure 6. Simulated elements efficiency of the proposed configurations and their average values (some values are overlapping).

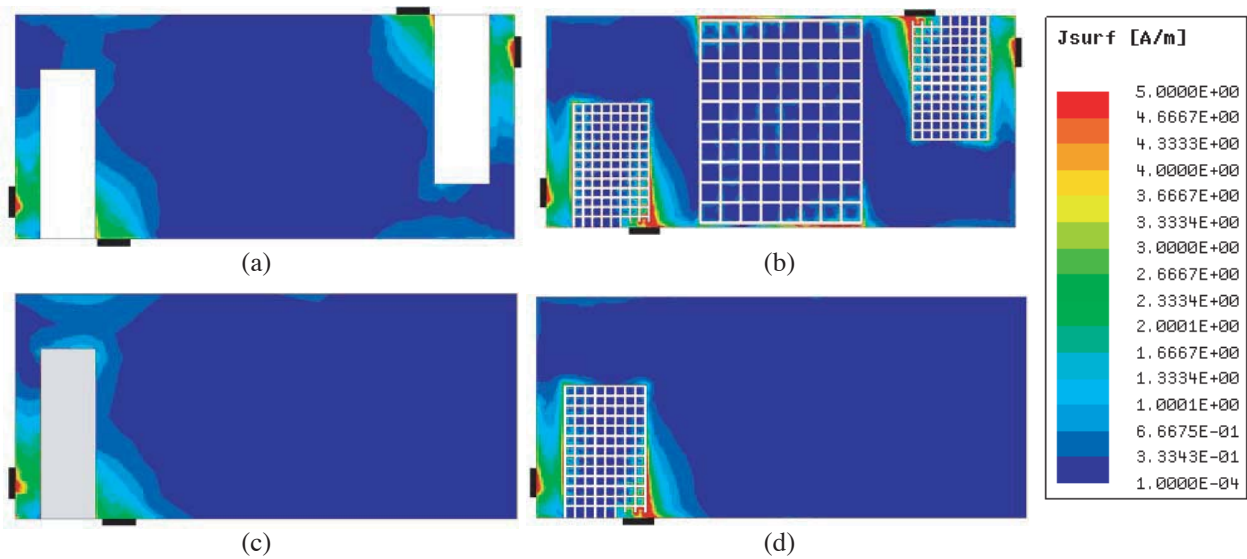


Figure 7. Surface current distribution of the ground plane for studied configurations at 3.5 GHz. (a) Configuration 1. (b) Configuration 2. (c) Configuration 3. (d) Configuration 4.

The CDF of relative signal-to-noise-ratio (SNR) for the four configurations were calculated using Eq. (9). These results are shown in Fig. 9. For comparison, the CDF considering the Rayleigh distribution is also included in Fig. 9. As seen, the CDFs of DGS ground configurations offer a better diversity performance than the ones without DGS ground where the CDF curves of DGS configurations were shifted to higher SNR values. This improvement of the diversity performance is attributed to the enhancement of the ports' efficiencies and the reduction of the correlation between the elements. The EDG at 1% outage probability was calculated using Eq. (8). The EDG values are 8.14 dB, 8.64 dB, 14.95 dB, and 15.98 dB for Configurations 1, 2, 3, and 4, respectively. The increase of the EDG for the configurations with DGS ground corresponds to the increase of the SNR which is translated on the system level to a reduction of the bit error rate (BER) or a reduction of the transmitted power of the diversity scheme without a performance loss. This can also alternately be used to increase the communication channel capacity in MIMO systems. Table 3 compares between the parameters of the proposed DGS configurations and other related studies in literature. As noted, this work offers superior performance in terms of efficiency, isolation, and EDG compared to the existing state-of-the-art.

Table 2. MEG and ECC values obtained from S-parameters and radiation patterns for the proposed configurations.

Parameter	Configuration 1		Configuration 2	
	<i>S</i> -parameters	patterns	<i>S</i> -parameters	patterns
MEG1	0.4475	0.4687	0.491000	0.4978
MEG2	0.4361	0.4566	0.492500	0.5086
ECC12	0.0165	0.0240	0.000004	0.0001
Parameter	Configuration 3		Configuration 4	
	<i>S</i> -parameters	patterns	<i>S</i> -parameters	patterns
MEG1 = MEG3	0.4091	0.443600	0.481700	0.47670
MEG2 = MEG4	0.4278	0.453900	0.480300	0.49230
ECC12 = ECC34	0.0611	0.023574	0.000005	0.00024
ECC14 = ECC23	0.0660	0.029459	0.000039	0.00017
ECC13	0.1579	0.006510	0.000060	0.00538
ECC24	0.1267	0.001569	0.000150	0.00012

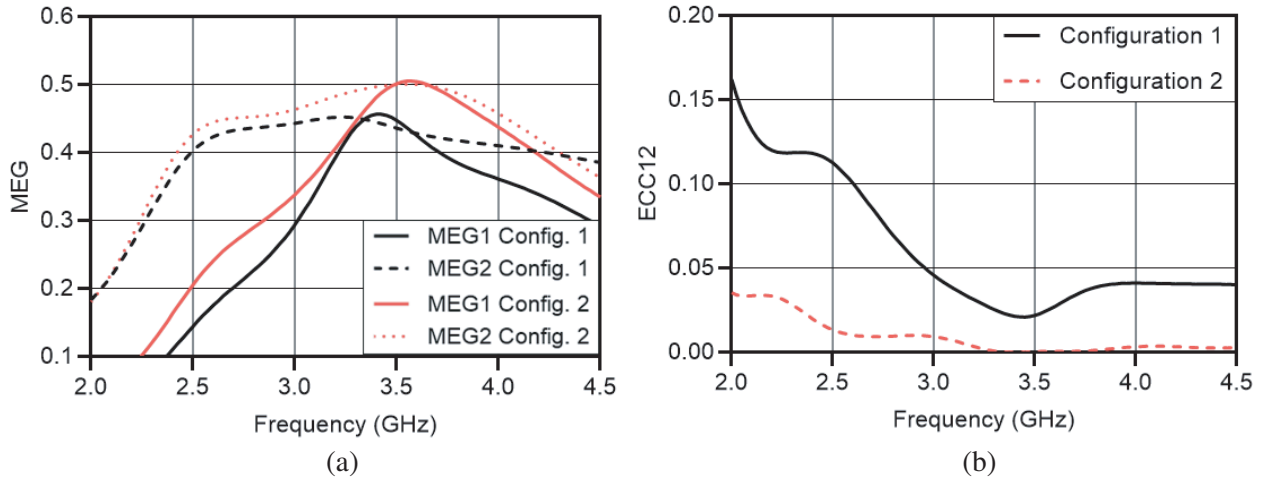


Figure 8. (a) Mean effective gain of ports for Configuration 1 and Configuration 2 over frequency. (b) Envelope correlation coefficient for Configuration 1 and Configuration 2 over frequency.

Table 3. Comparison between the parameters of the proposed MIMO antennas and related studies.

	Average ports efficiency (%)		Average isolation at resonance (dB)		EDG at 1% outage probability (dB)	
	2-ports	4-ports	2-ports	4-ports	2-ports	4-ports
Karaboikis et al. [21]	85	66	22	15	7.80	14.10
Chattha et al. [29]	96	N/A	15	N/A	7.20	N/A
Ghosh et al. [30]	N/A	79	N/A	14	N/A	14.96
Gago et al. [31]	N/A	76	N/A	14	9.69	14.78
This work (EBG designs)	98	96	27	25	8.64	15.98

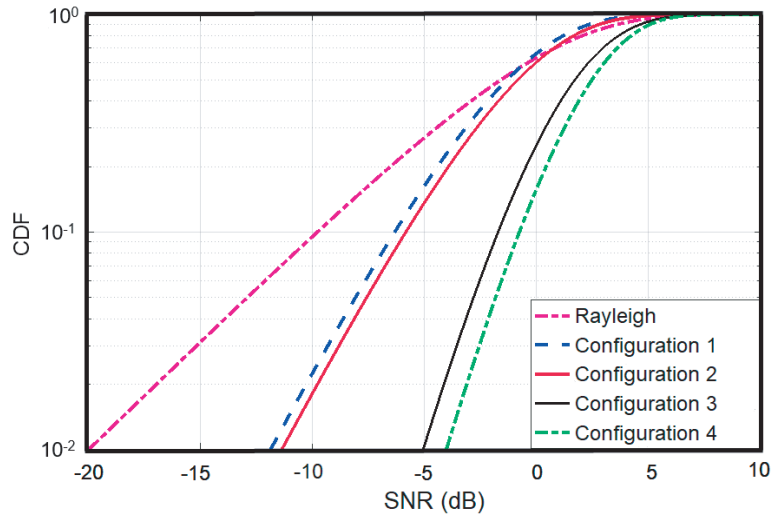


Figure 9. CDF of relative SNR for the investigated configurations.

5.2. MIMO Performance

The performance of a 2×2 and 4×4 MIMO system consisting of the proposed configurations was evaluated using Eq. (12). This was done using 50 000 channel realizations. The CDFs of relative capacity at 10 dB SNR of the studied configurations are shown in Fig. 10. As noted, the DGS configurations offer higher capacity than the ones without the DGS where the ergodic capacities are 5.28 bps/Hz, 5.51 bps/Hz, 10.11 bps/Hz, and 10.72 bps/Hz for configurations 1, 2, 3, and 4, respectively. This also validates the diversity results presented in Fig. 9. This capacity improvement can be attributed to the increase in the elements' efficiencies and the reduction in the correlation between the elements.

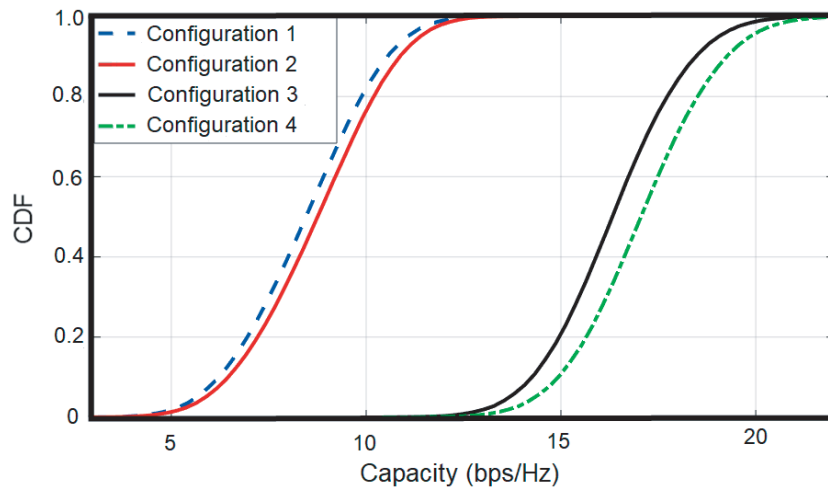


Figure 10. CDF of MIMO capacity of the investigated configurations at 10 dB SNR.

6. EFFECT OF USER PROXIMITY ON THE OPTIMUM MIMO ANTENNA PERFORMANCE

The body of a user impacts antenna performance due to its close proximity to the antenna, PCB, and housing. A considerable amount of power is absorbed by the human tissues. Antenna radiation efficiency is naturally degraded due to the lossy nature of the tissues. Since Configuration 4 yielded the

best MIMO performance, we decided to investigate it further in the presence of a user's hand and head. Studies were conducted using head and hand phantoms.

Two cases were considered: (1) data mode, in which the mobile is surrounded by a hand representing browsing and/or texting (2) voice mode, in which the mobile is close to the human head and carried by the hand representing conversation. The simulation models employed are depicted in Fig. 11. The hand and head were modeled as homogenous structures with the 'human average' material properties available within Ansys HFSS libraries. The hand and head effects on the antenna are summarized in columns 3 and 4 in Table 4. For comparison, results for the free-space case are listed in column 2. As observed, effects on the antenna impedance bandwidth ($S_{ii} < -10$ dB) and coupling are quite negligible. However, the MEG and EDG have degraded due to radiation efficiency degradation.

Simulated efficiencies for these various cases are shown in Fig. 12. The antenna ports in free space have the highest efficiency around 96% at 3.5 GHz. In the data mode, the average port efficiency decreases to around 50%. In the voice mode, port efficiency decreases to around 30%. Since mismatch

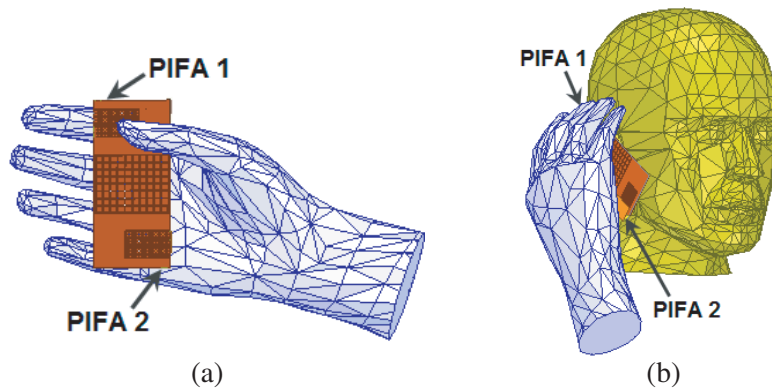


Figure 11. Models used to study the user effect on the MIMO antenna performance. (a) Data mode. (b) Voice mode.

Table 4. Head and hand effects on MIMO antenna performance.

	Free space	Data mode	Voice mode
port 1 Bandwidth	670 MHz 3.33 GHz to 4.00 GHz	720 MHz 3.40 GHz to 4.12 GHz	810 MHz 3.34 GHz to 4.15 GHz
port 2 Bandwidth	1420 MHz 2.68 GHz to 4.10 GHz	1000 MHz 3.35 GHz to 4.35 GHz	1060 MHz 3.34 GHz to 4.40 GHz
port 3 Bandwidth	670 MHz 3.33 GHz to 4.00 GHz	570 MHz 3.45 GHz to 4.02 GHz	500 MHz 3.35 GHz to 3.85 GHz
port 4 Bandwidth	1420 MHz 2.68 GHz to 4.10 GHz	1100 MHz 3.30 GHz to 4.40 GHz	650 MHz 3.25 GHz to 3.90 GHz
Average coupling at 3.5 GHz [dB]	-23.7	-19.9	-21.8
MEG1 at 3.5 GHz	0.4817	0.2534	0.1465
MEG2 at 3.5 GHz	0.4803	0.2478	0.1483
MEG3 at 3.5 GHz	0.4817	0.2552	0.1679
MEG4 at 3.5 GHz	0.4803	0.2615	0.1660
Average ECC	0.00005	0.00222	0.00152
EDG [dB]	15.98	13.20	11.12

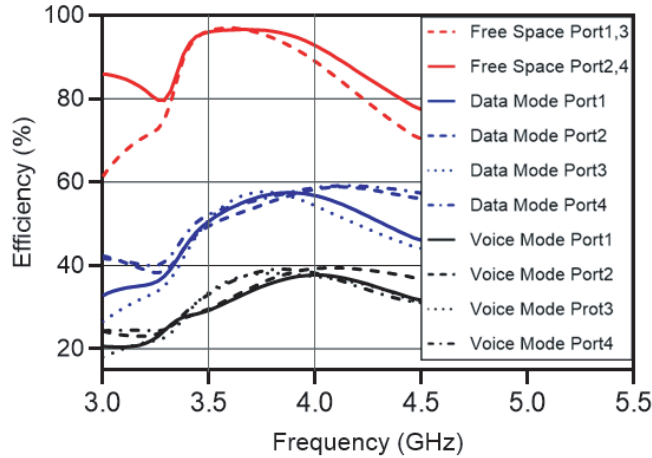


Figure 12. Simulated total ports efficiency for free space, data mode and voice mode.

loss is almost unchanged, the reduction in the efficiency can be attributed to the reduction in the radiation efficiency. It should be noted, however, that the efficiency numbers in the presence of the user will depend on the size of the hand, the distance of the device with respect to the head and hand, and how the device is hold or placed near the head or by the hand. Thus, efficiencies can improve depending on the circumstances mentioned.

Average port efficiencies at 3.5 GHz for Configuration 3 (4-port design without DGS) and Configuration 4 (4-port design with DGS) are compared in Table 5. It is shown that the design with the DGS ground exhibits better efficiency for the user proximity scenarios.

Table 5. Average ports efficiency (%) at 3.5 GHz for different scenarios.

	Configuration 3	Configuration 4
Free space	83.6	96.2
Data mode	44.1	50.4
Voice mode	25.1	31.4

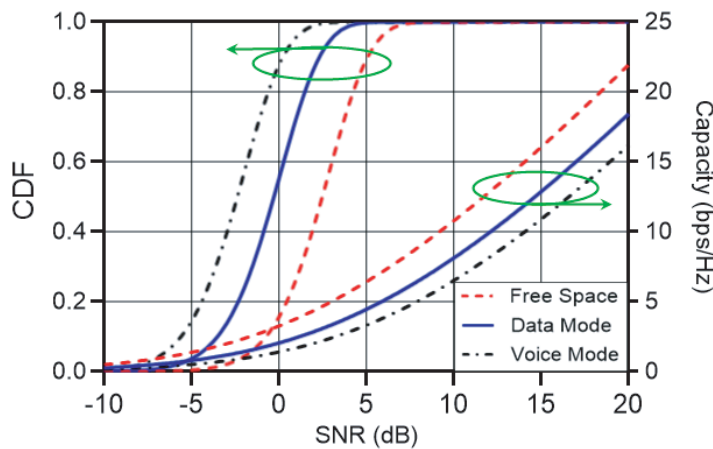


Figure 13. Effect of user proximity on the Diversity/MIMO performance of the antenna (Configuration 4).

The effect of the user on the diversity and MIMO performance of the antenna was also studied, and the results are shown in Fig. 13. As seen, the EDGs at 1% outage probability are 15.98 dB, 13.2 dB, 11.12 dB for free space, data mode, voice mode scenarios, respectively. Capacity analyses considering 10 00 channel realizations were also performed which shows that the system throughput at 10 dB SNR is 8.1 bps/Hz and 6.5 bps/Hz for data and voice modes, respectively compared to the free-space case of 10.7 bps/Hz. The capacity reduction is entirely due to the antenna efficiency reduction outlined in Fig. 12.

7. CONCLUSION

This paper presents the analysis of a two-port PIFA consisting of a new DGS design under MIMO configurations. It is shown that the proposed DGS design can significantly improve the port to port isolation of the two-port PIFA. This isolation improvement corresponds to an enhancement of the element's efficiency (efficiency increases by 15% over the antenna consisting of only a slot on the ground) and MIMO capacity. Among the studied configurations, the two PIFAs with the DGS (Configuration 4) achieve nearly 16 dB EDG at 1% outage probability and offer 10.72 bps/Hz capacity at 10 dB SNR. The performance of the proposed configuration is also superior to the traditional slot only on the ground configuration in the voice and data modes.

REFERENCES

1. Hussain, R., A. T. Alreshaid, S. K. Podilchak, and M. S. Sharawi, "Compact 4G MIMO antenna integrated with a 5G array for current and future mobile handsets," *IET Microw., Antennas Propag.*, Vol. 11, No. 2, 271–279, 2017.
2. Kildal, P. S. and K. Rosengren, "Correlation and capacity of MIMO systems and mutual coupling, radiation efficiency and diversity gain of their antennas: Simulations and measurements in a reverberation chamber," *IEEE Commun. Mag.*, Vol. 42, No. 12, 104–112, Dec. 2004.
3. Zhao, A. and Z. Ren, "Size reduction of self-isolated MIMO antenna system for 5G mobile phone applications," *IEEE Antennas Wireless Propag. Lett.*, Vol. 18, No. 1, 152–156, Jan. 2019.
4. Abdelgwad, A. H. and M. Ali, "A new pattern and polarization diversity MIMO antenna for handheld devices," *IEEE Int. Sympos. Antennas Propag. (APS)*, Montreal, Canada, 2020.
5. Deng, J., J. Li, L. Zhao, and L. Guo, "A dual-band inverted-F MIMO antenna with enhanced isolation for WLAN applications," *IEEE Antennas Wirel. Propag. Lett.*, Vol. 61, 2270–2273, 2018.
6. Jiang, W., Y. Cui, B. Liu, W. Hu, and Y. Xi, "A dual-band MIMO antenna with enhanced isolation for 5G smartphone applications," *IEEE Access*, Vol. 7, 112554–112563, 2019.
7. Luo, C., J. Hong, and L. Zhong, "Isolation enhancement of a very compact UWB-MIMO slot antenna with two defected ground structures," *IEEE Antennas Wirel. Propag. Lett.*, Vol. 14, 1766–1769, Apr. 2015.
8. Li, M., Y. Ban, Z. Xu, J. Guo, and Z. Yu, "Tri-polarized 12 antenna MIMO array for future 5G smartphone applications," *IEEE Access*, Vol. 6, 6160–6170, 2018.
9. Chen, X., S. Zhang, and Q. Li, "A review of mutual coupling in MIMO systems," *IEEE Access*, Vol. 6, 24706–24719, 2018.
10. Abdelgwad, A. H. and M. Ali, "Isolation improvement between closely-spaced antennas using EBG," *Int. Applied Comput. Electromagn. Society (ACES) Sympos.*, Monterey, USA, 2020.
11. Abdelgwad A. H. and M. Ali, "Mutual coupling reduction of a two-element MIMO antenna system using defected ground structure," *IEEE Int. Sympos. Antennas Propag (APS)*., Montreal, Canada, 2020.
12. Al-Hassan, M. J., T. A. Denideni, and A. R. Sebak, "Millimeter-wave compact EBG structure for mutual coupling reduction applications," *IEEE Trans. Antennas Propag.*, Vol. 63, No. 2, 823–828, Feb. 2015.
13. Mavridou, M., A. P. Feresidis, and P. Gardner, "Tunable double-layer EBG structures and application to antenna isolation," *IEEE Trans. Antennas Propag.*, Vol. 64, No. 1, 70–79, Jan. 2016.

14. Abdelgwad, A. H. and M. Ali, "Isolation improvement of a two-port PIFA for MIMO using a planar EBG ground," *Microw. Opt. Technol. Lett.*, Vol. 62, No. 2, 737–742, Feb. 2020.
15. Li, Y., C. Sim, Y. Luo, And G. Yang, "12-port 5G massive MIMO antenna array insub-6 GHz mobile handset for LTE bands 42/43/46 applications," *IEEE Access*, Vol. 6, 344–354, 2018.
16. Abdelgwad A. H. and M. Ali, "Printed dipole MIMO antenna for wireless handheld terminals," *14th European Conf. Antennas Propag. (EuCAP)*, Copenhagen, Denmark, 2020.
17. Meshram, M. K., R. K. Animeh, A. T. Pimpale, and N. K. Nikolova, "A novel quad-band diversity antenna for LTE and Wi-Fi applications with high isolation," *IEEE Trans. Antennas Propag.*, Vol. 60, No. 9, 4360–4371, Sept. 2012.
18. Chattha, H. T., M. Nasir, Q. H. Abbasi, Y. Huang, and S. S. AlJa'afreh, "Compact low-profile dual-port single wideband planar inverted-F MIMO antenna," *IEEE Antennas Wirel. Propag. Lett.*, Vol. 12, 1673–1975, Dec. 2013.
19. Chattha H. T., "4-port 2-element MIMO antenna for 5G portable applications," *IEEE Access*, Vol. 7, 95616–95620, 2019.
20. Taga, T., "Analysis for mean effective gain for mobile in land mobile radio environments," *IEEE Trans. Veh. Technol.*, Vol. 39, No. 2, 117–131, May 1990.
21. Karaboikis, M., V. Papamichael, G. Tsachtsiris, C. Soras, and V. Makios, "Integrating compact printed antennas onto small diversity/MIMO terminals," *IEEE Trans. Antennas Propag.*, Vol.56, No. 7, 2067–2078, Jul. 2008.
22. Taga, T., "Analysis of correlation characteristics of antenna diversity in land mobile radio environments," *Electron. Commun. Jpn.*, Vol. 74, No. 8, Pt. 1, 101–115, 1991.
23. Jensen, M. A. and Y. R. Samii, "Performance analysis of antennas for hand-held transceivers using FDTD," *IEEE Trans. Antennas Propag.*, Vol. 42, 1106–1113, Aug. 1994.
24. Stjernman, A., "Relationship between radiation pattern correlation and scattering matrix of lossless and lossy antennas," *Electron. Lett.*, Vol. 41, No. 12,678–680, 2005.
25. Takada, J. and K. Ogawa, "Concept of diversity antenna gain," Paris, France, EURO-COST 273 TD (3) 142, 2003.
26. Chen, X., P. Kildal, and J. Carlsson, "Simple calculation of ergodic capacity of lossless two-port antenna system using only S -parameters — Comparison with common Z -parameter approach," *IEEE Int. Sympos. Antennas Propag.*, Spokane, USA, 2011.
27. Ozdemir, M. K., E. Arvas, and H. Arslan, "Dynamics of spatial correlation and implications on MIMO systems," *IEEE Commun. Mag.*, Vol. 42, No. 6, S14–S19, Jun. 2004.
28. Song, H. J., A. Bekaryan, J. H. Schaffner, A. Hussain, and P. Kildal, "Effects of mutual coupling on LTE MIMO capacity for monopole array: Comparing reverberation chamber tests and drive tests," *IEEE Antennas Wirel. Propag. Lett.*, Vol. 14, 474–457, Nov. 2014.
29. Chattha, H. T., Y. Huang, S. J. Boyes, and X. Zhu, "Polarization and pattern diversity-based dual-feed planar inverted-F antenna," *IEEE Trans. Antennas Propag.*, Vol. 60, No. 3, 1532–1539, Mar. 2012.
30. Ghosh, S., T. Tran, and T. Le-Ngoc, "Miniaturized four-element diversity PIFA," *IEEE Antennas Wirel. Propag. Lett.*, Vol. 12, 396–400, 2013.
31. Gago, O., L. González, and R. Eickhoff, "Study of the optimum number of radiating elements for different portable devices operating in a MIMO system," *European Wirel. Conf.*, Aalborg, Denmark, 2009.